Reduction of skylight reflection effects in the above-water measurement of diffuse marine reflectance

Bertrand Fougnie, Robert Frouin, Pierre Lecomte, and Pierre-Yves Deschamps

Reflected skylight in above-water measurements of diffuse marine reflectance can be reduced substantially by viewing the surface through an analyzer transmitting the vertically polarized component of incident radiance. For maximum reduction of effects, radiometric measurements should be made at a viewing zenith angle of ~45° (near the Brewster angle) and a relative azimuth angle between solar and viewing directions greater than 90° (backscattering), preferably 135°. In this case the residual reflected skylight in the polarized signal exhibits minimum sensitivity to the sea state and can be corrected to within a few 10^{-4} in reflectance units. For most oceanic waters the resulting relative error on the diffuse marine reflectance in the blue and green is less than 1%. Since the water body polarizes incident skylight, the measured polarized reflectance differs from the total reflectance. The difference, however, is small for the considered geometry. Measurements made at the Scripps Institution of Oceanography pier in La Jolla, Calif., with a specifically designed scanning polarization radiometer, confirm the theoretical findings and demonstrate the usefulness of polarization radiometry for measuring diffuse marine reflectance.

OCIS codes: 260.5430, 010.4450, 290.1310, 120.6660, 120.5700, 240.0240.

1. Introduction

Accurate field measurements of diffuse marine reflectance, or the radiance backscattered by the ocean normalized to the incident solar irradiance, times π, are necessary to check the calibration of satellite ocean-color sensors while they operate in orbit and evaluate schemes that correct atmospheric and surface effects in the satellite data (e.g., Refs. 1–3). The measurements are not made directly but through upwelled and downwelled components. Underwater instrumentation is traditionally used, such as the MER class of radiometer, and the upwelled radiance and downwelled irradiance data acquired at depth are extrapolated to the surface and propagated upward through the interface. The incident solar irradiance above the surface is also measured directly, in most cases with standard pyranometers. Accuracy in the surface quantities depends on exposure errors (e.g., ship shadow and instrument self-shading) and uncertainties in the extrapolation scheme. In turbid waters, or in the red, where the absorption coefficient is large, the extrapolation to the surface may be particularly difficult.[4]

In part, because of inherent difficulties in underwater techniques, above-water techniques have been developed as an alternative for measuring diffuse marine reflectance (e.g., Refs. 5 and 6). In these techniques the ocean surface is viewed radiometrically at a nadir angle of 30° and a relative azimuth angle between solar and viewing directions of 90°. Normalization to incident solar irradiance is performed by measuring the radiance reflected by a diffuse plaque of known optical properties, positioned horizontally in front of the radiometer. The reference target is sampled at a right angle unless there is an instrument shadow. A major problem, however, is removing the effect of skylight reflection by the wavy interface and eventually residual sun glint. In the quick-and-easy procedure of Carder and Steward,[5] reflected skylight is removed by subtracting the sky radiance measured at 30° from zenith (i.e., in the direction of the skylight reflected into the sensor by a

When this study was performed, B. Fougnie, P. Lecomte, and P.-Y. Deschamps were with the Laboratoire d'Optique Atmospherique, Universite des Sciences et Technologies de Lille, 59655 Villeneuve d'Ascq, France. Their e-mail addresses are lecomte@loa.univ-lille1.fr and deschamps@loa.univ-lille1.fr. B. Fougnie is now with the Centre National d'Etudes Spatiales, 18 avenue E. Belin, 31401 Toulouse, France. His e-mail address is bertrand.fougnie@cnes.fr. R. Frouin is with the Scripps Institution of Oceanography, University of California, San Diego, 9500 Gilman Drive, La Jolla, California 92093-0221. His e-mail address is frouin@genius.ucsd.edu.

Received 22 September 1998; revised manuscript received 3 February 1999.

0003-6935/99/183844-13$15.00/0

flat surface), after multiplication by the Fresnel coefficient at the same angle. The residual sun glint at any visible wavelength is derived by assuming that the water-leaving radiance at 750 nm is equal to zero.

As pointed out by Lee *et al.*,[6] one difficulty with the quick-and-easy procedure is that, owing to the uneven surface, the skylight reflected into the sensor may originate from a large solid angle. Furthermore in turbid waters the water-leaving radiance at 750 nm may not be close to zero. For better correction of the reflected skylight, Lee *et al.*[6] partitioned the skylight into molecular and aerosol contributions, removed the molecular contribution by using an average Fresnel coefficient, and estimated the aerosol contribution by using an optimization algorithm. Carder *et al.*,[7] on the other hand, used a vertical polarizer in front of the radiance sensor to reduce the reflected skylight. Since reflected sunlight is polarized horizontally at the Brewster angle, one expects that radiance measurements obtained with a vertical polarizer near that angle will be minimally affected by reflected sunlight. Lee *et al.*[8] compared the two types of measurements but could not evidence any improvement in the accuracy of diffuse marine reflectance by using a vertical polarizer. Polarized and unpolarized measurements made both at a viewing zenith angle of 30° and at a relative azimuth angle of 90° yielded close results. The lack of improvement, however, might be due to the viewing angle selected (30°), which was far from the Brewster angle (53°), but could also be attributed to the loss of blue signal by the polarizer. Furthermore the hyperspectral radiometer used by Lee *et al.*[8] has several optical elements that may enhance or degrade polarizer radiance.

In this paper the effects of skylight reflection on measurement of diffuse marine reflectance from above the surface are investigated theoretically as a function of solar and viewing angles, atmospheric conditions, and sea state. Improvements from using a vertical polarizer are quantified, and the optimum geometries to minimize the reflected skylight are identified. We verified the theoretical findings experimentally at the Scripps Institution of Oceanography (SIO) pier by viewing the ocean surface with a specifically designed, scanning polarization radiometer. Recommendations are made about the adequacy of polarization radiometry for routine measurements of diffuse marine reflectance.

2. Theory

The radiance L_0 measured by a radiometer viewing the ocean above the surface can be considered as the sum of two components: (1) a radiance due to backscattering by the water body L_w^+, otherwise known as the water-leaving radiance, and (2) a radiance due to the Fresnel reflection of the downward solar irradiance at the air–sea interface L_c. Thus the observed radiance can be written

$$L_0(\lambda, \theta_s, \theta_v, \varphi) = L_w^+(\lambda, \theta_s, \theta_v, \varphi) + L_c(\lambda, \theta_s, \theta_v, \varphi), \quad (1)$$

where θ_v is the viewing zenith angle, θ_s is the solar zenith angle, φ is the azimuth angle relative to the solar plane, and λ is the wavelength, hereafter omitted for clarity. Neglecting the radiance due to surface whitecaps (wind speeds of less than 5 m s^{-1} (Ref. 9), the radiance L_c can be written

$$L_c(\theta_s, \theta_v, \varphi) = L_s(\theta_s, \theta_v, \varphi) + L_g(\theta_s, \theta_v, \varphi), \quad (2)$$

where L_g is the radiance due to reflection of the direct solar irradiance on the sea surface, called glitter, and L_s is the radiance due to reflection of the diffuse solar irradiance or sky radiance. In Eq. (1) the interaction between water-leaving radiance and atmospheric scatterers, whose effect on L_0 is small, has been neglected. In Eq. (2) the radiance L_g includes the interaction between the glitter radiance and molecules/aerosols, a process that cannot be neglected. The radiance L_w^+ is the component of interest for bio-optical applications, and L_c therefore is a perturbation that needs to be corrected, hence estimated accurately.

For a specular reflection of the sky radiance at the air–sea interface (the flat ocean surface) L_s is simply the downward radiance L_s^d in the specular direction, multiplied by the Fresnel reflection coefficient. The parallel-polarized component of L_s, however, becomes nil at the Brewster viewing angle, i.e., at 53° for a water–air refractive index of 1.33. Thus at this angle L_s is totally perpendicular polarized and can be completely eliminated by use of a polarizer. When viewing the sea surface, the parallel axis is the intersection between the vertical plane (containing vertical and viewing directions) and the vibration plane (perpendicular to the viewing direction). The perpendicular axis is perpendicular to both the parallel axis and the viewing direction and therefore is horizontal.

In reality, the reflection is not specular because of the wavy surface. The ocean surface, however, can be considered as a sum of small planes with an orientation described statistically by Cox and Munk[10] and for which reflection is assumed to be specular. The reflected radiance L_s therefore no longer depends on the downward radiance L_s^d in the specular direction but on the downward radiance in a finite solid angle around the specular direction. The more agitated the surface, the wider the solid angle. This can be written as

$$L_s(\theta_s, \theta_v, \varphi) = \int_0^{2\pi} \int_0^{\pi/2} L_s^d(\theta, \theta_s, \varphi) p(V, \theta_v, \theta, \varphi) \times p(V, \theta_v, \theta, \varphi) r(\theta_v, \theta, \varphi) \sin(\theta)\cos(\theta) d\theta d\varphi, \quad (3a)$$

where $r(\theta_v, \theta_s, \varphi)$ is the Fresnel reflection coefficient corresponding to the geometry $(\theta_v, \theta_s, \varphi)$, and $p(V, \theta_v, \theta_s, \varphi)$ is the probability (in s rad^{-1}) for the incident ray, with a zenith angle of θ, to be reflected in the viewing zenith angle θ_v by the surface of roughness characterized by wind speed V.[10] In Eq. (3a) L_s^d can

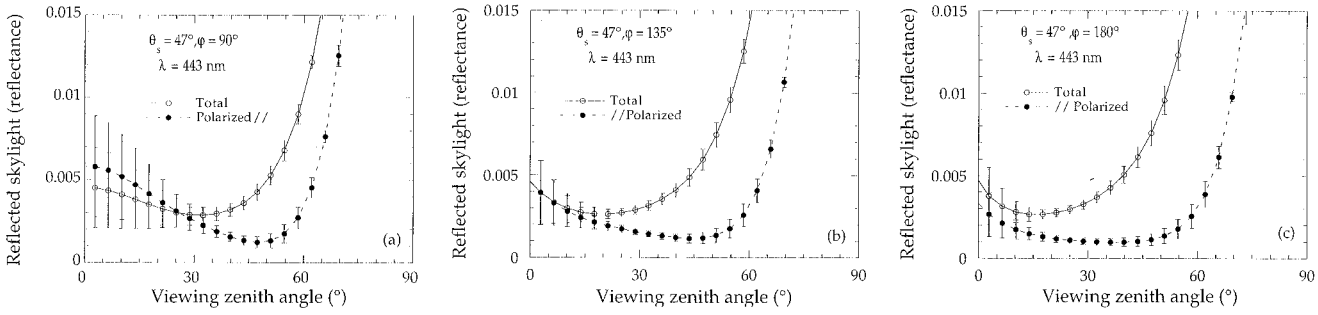

Fig. 1. Parallel-polarized (dots) and total (circles) reflectances of the ocean at 443 nm computed as a function of the viewing zenith angle for three relative azimuth angles: (a) 90°, (b) 135°; and (c) 180°. The solar zenith angle is 47°. The water-body reflectance is assumed to equal zero and the atmosphere contains only molecules. The error bar represents the minimum and the maximum values for varied wind speeds from 2 to 12.5 m s^{-1}.

be computed from the optical properties of the atmospheric constituents (molecules and aerosols) and their vertical distribution.

The glitter radiance L_g in Eq. (2), due to reflection of the direct solar irradiance at the ocean surface, can be written

$$L_g(\theta_s, \theta_v, \varphi) = E_{so}\cos(\theta_s)\exp\left[-\frac{\delta}{\cos(\theta_s)}\right] \times p(V, \theta_v, \theta_s, \varphi)r(\theta_v, \theta_s, \varphi), \quad (3b)$$

where E_{so} is the extraterrestrial solar irradiance, $p(V, \theta_v, \theta_s, \varphi)$ is the probability defined in Eq. (3a), and δ is the atmospheric optical depth. It is convenient to normalize the radiance observed at the bottom of the atmosphere L_0 in Eq. (1) and the reflected radiance L_c to the solar irradiance at the top of the atmosphere and to express them in terms of reflectance according to

$$\rho_{0,c}(\theta_s, \theta_v, \varphi) = \frac{\pi L_{0,c}(\theta_s, \theta_v, \varphi)d^2}{\cos(\theta_s)E_{so}{d_0}^2}, \quad (4)$$

where E_{so} is the extraterrestrial solar irradiance perpendicular to a plane surface at the mean Sun–Earth distance of d_0 and d is the Sun–Earth distance at the time of the measurement. Introducing polarized components of ρ_0 and ρ_c by normalizing the polarized components of radiances L_0 and L_c to half of the solar irradiance at the top of the atmosphere E_{s0} considered unpolarized, we have

$${\rho_{o,c}}^{//,\perp}(\theta_s, \theta_v, \varphi) = \frac{2\pi {L_{0,c}}^{//,\perp}(\theta_s, \theta_v, \varphi)d^2}{\cos(\theta_s)E_{s0}{d_0}^2}. \quad (5)$$

Consequently Eq. (1) becomes

$$\rho_0(\theta_s, \theta_v, \varphi) = {\rho_c}^{//}(\theta_s, \theta_v, \varphi) + {\rho_c}^{\perp}(\theta_s, \theta_v, \varphi) + t_a(\theta_s){\rho_w}^{+}(\theta_s, \theta_v, \varphi), \quad (6)$$

where t_a is the atmospheric transmittance, sum of direct and diffuse components, and ${\rho_w}^{+}$ is the diffuse marine reflectance, i.e., the water-leaving radiance ${L_w}^{+}$ multiplied by π and normalized to the solar irradiance at the bottom of the atmosphere. Therefore ${\rho_w}^{+}$ can be expressed as

$${\rho_w}^{+}(\theta_s, \theta_v, \varphi) = \frac{\rho_o(\theta_s, \theta_v, \varphi) - \rho_c(\theta_s, \theta_v, \varphi)}{t_a(\theta_s)} \quad (7a)$$

or, when polarized components are used,

$${\rho_w}^{+}(\theta_s, \theta_v, \varphi) = \frac{{\rho_o}^{//}(\theta_s, \theta_v, \varphi) - {\rho_c}^{//}(\theta_s, \theta_v, \varphi)}{t_a(\theta_s)}, \quad (7b)$$

where ${\rho_c}^{//}$ is a term that must be determined to retrieve the diffuse marine reflectance. The estimation of ${\rho_w}^{+}$ in Eq. (7b) assumes that the radiance scattered by the ocean is unpolarized.

Computations of ρ_c and its polarized components were made for various geometric, atmospheric, and surface conditions by use of the successive orders of scattering code of Deuzé *et al.*[11] The water body reflectance was assumed to be equal to zero. Surface roughness was parameterized as a function of wind speed, following Cox and Munk,[10] and wind speed was varied from 2 to 12.5 m s^{-1}. Solar zenith angles of 32°, 47°, and 58°; relative azimuth angles of 90°, 135°, and 180° (backscattering); and viewing zenith angles ranging from 2° to 88° were used in the calculations. The atmosphere contained either molecules only or molecules and aerosols (aerosol optical depths of 0.1 and 0.2 at 865 nm).

The results are summarized in Figs. 1–5, which present the total reflectance, ρ_c and its parallel-polarized component ${\rho_c}^{//}$ as a function of the viewing zenith angle. The parallel-polarized component is expected to be reduced due to Fresnel reflection at the interface and therefore is the component to compare with ρ_c. According to the definition of polarized components [Eqs. (4) and (5)], ${\rho_c}^{//} > \rho_c$ means that the parallel-polarized component of the reflectance is larger than the perpendicular-polarized component. Average values over the range of selected wind speeds are displayed in the figures, and the error bars represent the minimum and the maximum values of ρ_c and ${\rho_c}^{//}$ for those wind speeds.

In Fig. 1 ρ_c and ${\rho_c}^{//}$ at 443 nm are displayed as a function of the viewing zenith angle for relative azimuth angles of 90° [the plane perpendicular to the

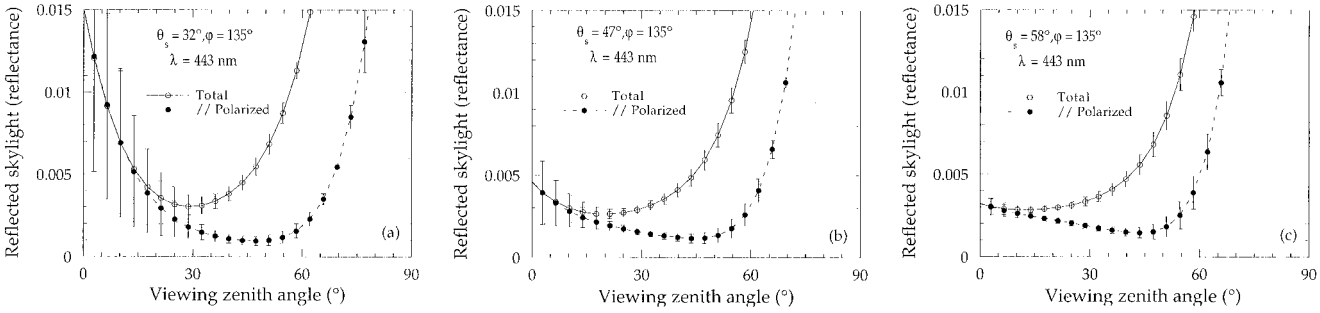

Fig. 2. Same as Fig. 1 but for a relative azimuth angle of 135° and for three solar zenith angles: (a) 32°, (b) 47°, and (c) 58°.

solar plane, Fig. 1(a), 135° [Fig. 1(b)], and 180° [solar plane, Fig. 1(c)] and for an atmosphere containing only molecules. Skylight reflection and glitter effects are reduced substantially in the polarized component near the Brewster angle with minimum values observed near 45°. At this viewing angle, $\rho_c^{//}$ is ~0.001 compared with 0.004–0.006 for ρ_c. Because the surface is not flat, the minimum values of $\rho_c^{//}$ are not obtained at exactly the Brewster angle but at a smaller angle (~45°). As the relative azimuth angle increases, $\rho_c^{//}$ also becomes minimum near a 45° viewing zenith angle and remains smaller than ρ_c. At small viewing zenith angles (<30°) the influence of glitter makes both the total and the polarized component of ρ_c strongly dependent on wind speed, especially when the relative azimuth angle is 90°. This strong dependence indicates that accurate correction of skylight reflection and glitter effects in measurements of water-leaving radiance made at a 30° viewing zenith angle and a 90° relative azimuth angle and without a polarizer[6,7] requires precise knowledge of the wind speed. Variability due to wind speed, on the other hand, can be neglected by use of a polarizer and viewing the surface at a 45° zenith angle.

When the solar zenith angle is increased from 32° to 58° (Fig. 2) both ρ_c and $\rho_c^{//}$ are much less influenced by wind speed below viewing zenith angles of 30°. Again the minimum value of $\rho_c^{//}$ is obtained near a 45° viewing zenith angle, but the values do not vary significantly from 10° to 55° when the relative azimuth angle is 180°. Note that the values of ρ_c and $\rho_c^{//}$ are similar at a 30° viewing zenith angle in the plane perpendicular to the Sun, which may explain, at least partly, why Lee *et al.*[8] found no significant differences in above-water measurements of diffuse marine reflectance made with and without a vertical polarizer. Using a polarizer and measuring at a 45° viewing zenith angle, however, one reduces the skylight reflection and glitter effects by factors of 3–4, depending on the solar zenith angle.

In Figs. 3(a), 3(b), and 3(c), ρ_c and $\rho_c^{//}$ are displayed for wavelengths of 443, 565, and 865 nm, respectively. The solar zenith angle is 47°, the relative azimuth angle is 135°, and as in Figs. 1 and 2 the atmosphere contains only molecules. For a fixed viewing zenith angle, both ρ_c and $\rho_c^{//}$ decrease with increasing wavelength, because molecular scattering is less efficient at longer wavelengths. (The diffuse part of incident irradiance at the surface is smaller.) At 865 nm the glitter contribution dominates ρ_c and $\rho_c^{//}$ below the 30° viewing zenith angle, and the effect, white spectrally, is also present at the other wavelengths, explaining the similarity in shape of the spectral dependence of ρ_c and $\rho_c^{//}$. Note that at 865 nm the reflected skylight signal is practically eliminated between the 30° and the 50° viewing zenith angle, which may be useful in detecting the presence of whitecaps and other anomalies (clouds) in measurements at shorter wavelengths.

The presence of aerosols (Figs. 4 and 5) increases both ρ_c [Figs. 4(a) and 5(a)] and $\rho_c^{//}$ [Figs. 4(b) and 5(b)], but the increase is much less for $\rho_c^{//}$ and is minimum around the 45° viewing zenith angle. The aerosol effect in ρ_c is reduced by factors of 3–4 in $\rho_c^{//}$ at this angle. More variability due to the aerosol

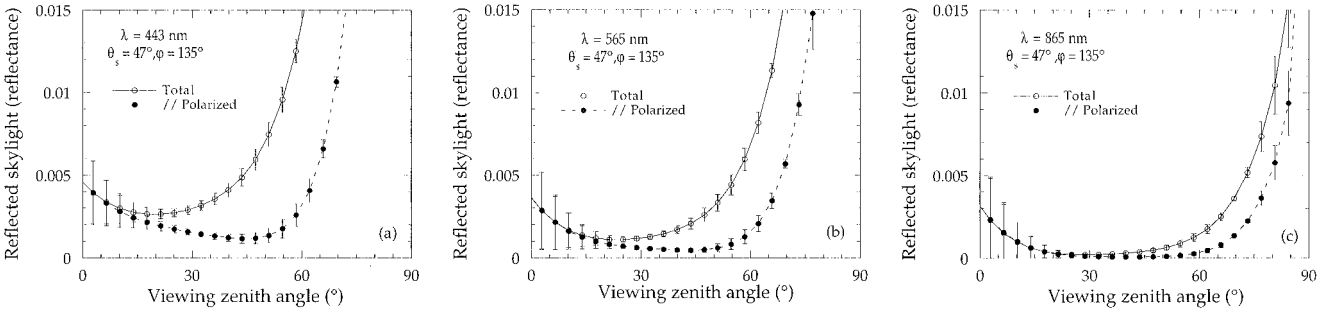

Fig. 3. Same as Fig. 1 but for a relative azimuth angle of 135°, a solar zenith angle of 47°, and for three wavelengths: (a) 443 nm, (b) 565 nm, and (c) 865 nm.

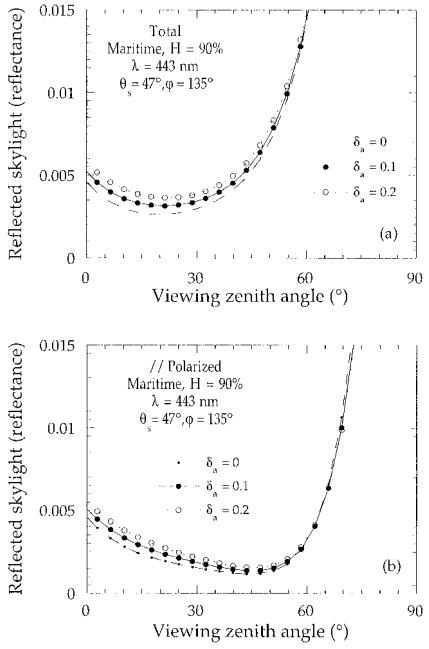

Fig. 4. (a) Total and (b) parallel-polarized reflectances of the ocean at 443 nm as a function of the viewing zenith angle for a solar zenith angle of 47° and a relative azimuth angle of 135°. The atmosphere contains maritime aerosols characterized by their optical depth at 865 nm (0.0.1 and 0.2) and the atmospheric relative humidity (90%).

amount is observed for maritime aerosols (Fig. 4) than for coastal-type aerosols (Fig. 5), but the effect on $\rho_c^{//}$ at a 45° viewing zenith angle can be neglected for practical purposes.

Based on the above simulations, an estimate of the budget error on the retrieval of marine reflectance

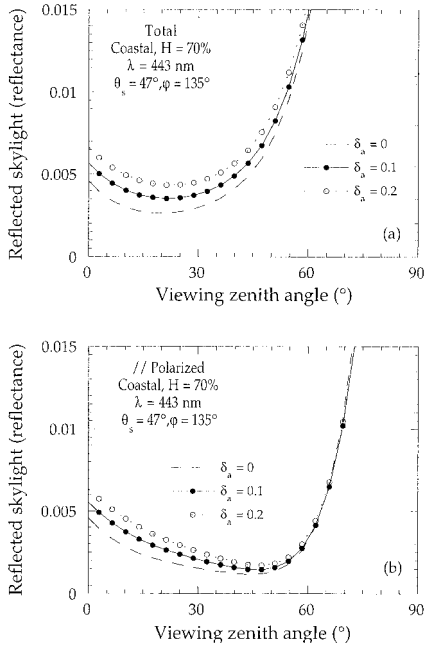

Fig. 5. Same as Fig. 4 but for a coastal aerosol with an atmospheric relative humidity of 70%.

Table 1. Error Budget (in Reflectance Units) on Diffuse Marine Reflectance Derived from Two Types of Measurement, at 443 and 565 nm, and for Several Solar Zenith Angles θ_s

θ_s (deg)	Parallel-Polarized $\theta_v = 45°$, $\varphi = 135°$		Unpolarized $\theta_v = 30°$, $\varphi = 90°$	
	443 nm	565 nm	443 nm	565 nm
32	0.00032	0.00023	0.00279	0.00304
47	0.00041	0.00025	0.00101	0.00093
58	0.00055	0.00033	0.00089	0.00080

has been derived, owing to uncertainties on the skylight reflection correction under clear sky. The two viewing geometries of interest were considered, namely, unpolarized measurements at a viewing zenith angle of 30° and a relative azimuth angle of 90° and parallel-polarized at a viewing zenith angle of 45° and a relative azimuth angle of 135°. The following assumptions were made: (1) the mean wind speed is 8.75 m s^{-1} and known with an accuracy of ± 2.5 m s^{-1}, (2) the aerosol optical thickness is 0.1 at 865 nm and known with an accuracy of ± 0.05, and (3) the azimuth and zenith angles of the measurements are known with an accuracy of $\pm 5°$. The error on the retrieved marine reflectance $\Delta\rho_w^{+}$ is computed by use of

$$\Delta\rho_w^{+}(\theta_s, \theta_v, \varphi) = \frac{\Delta\rho_c(\theta_s, \theta_v, \varphi)}{t_a(\theta_s)}, \tag{8}$$

where t_a is the diffuse atmospheric transmission defined in Eq. (6), which, when the effect of aerosols and gaseous absorption is neglected, is approximated by

$$t_a(\theta_s) \cong \exp\left[-\frac{0.48\delta_r}{\cos(\theta_s)}\right], \tag{9}$$

where δ_r is the atmospheric optical depth of molecules.[12] In Table 1 we give the quadratic sum of the four errors at 443 and 565 nm for the two types of measurements. At high solar elevations or low solar zenith angles the parallel-polarized method is very efficient—nearly 10 times more accurate than the unpolarized method at 443 nm, mainly because of its greater efficiency in eliminating glitter. At a low solar elevation or high solar zenith angles, the best accuracy again is obtained with the polarized method, but the improvement is smaller. Similar behavior can be observed at 565 nm but with smaller errors. Thus above-water polarized measurements should allow one to achieve a reduction of skylight reflection effects and a retrieval of diffuse marine reflectance with an accuracy better than 0.001 for most experimental conditions, an accuracy not achieved by above-water unpolarized measurements.

In summary, simulations of ρ_c and $\rho_c^{//}$ indicate that viewing the ocean surface radiometrically at 45° from zenith with a vertical polarizer should reduce dramatically the perturbing skylight reflection and glitter effects in measurements of water-leaving radiance or diffuse marine reflectance by typical factors

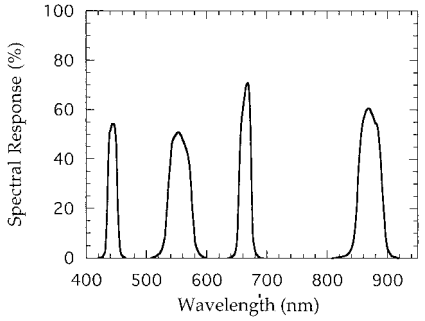

Fig. 6. Spectral response of the Refpol interference filters.

of 4–5. Since the residual effects are much smaller, they can be corrected more easily, all the more as the impact of wind speed and aerosols is minimized. Based on the analyses of Figs. 1–5, the choice of relative azimuth angle between 90° and 180° is not an issue. The residual effects are very close in the entire angular range. However, shadows might be a problem at large relative azimuth angles, while the minimum skylight reflection and glitter effects occur over a much shorter range of viewing zenith angles at small relative azimuth angles, and uncertainties in the viewing zenith angle might be significant. Furthermore glitter effects are more likely to contaminate the measurements at small relative azimuth angles when the solar zenith angle is small. It appears therefore that a relative azimuth angle of 135° is a good compromise.

3. Experimental Verification

A. Instrumentation

Spectral water-leaving radiance was measured with a polarization scanning radiometer (Refpol) designed by and built at the Laboratoire d'Optique Atmosphérique (LOA) of the University of Lille, France. This radiometer is composed of an optical head mounted on a scanner and executing a revolution (360°) in a vertical plane perpendicular to the horizontal rotating axis of the scanner. An inclinometer attached to the optical head measures the viewing zenith angle. The optical head and the scanner are connected to a PC for control of the system and data acquisition.

The optical head has four collimators fitted with interference filters. The central wavelengths of the filters are 443, 550, 665, and 870 nm (Fig. 6). The total field of view is 2° (see Table 2 for Refpol characteristics). Behind the interference filters are silicon photodiodes, a separate photodiode for each filter. Between the filters and the detectors a rotating wheel bears polarizer sheets separated by a band of optically black material (Fig. 7). One of the polarizer sheets is suitable for 443-, 550-, and 665-nm filters, the other for the 870-nm filter. The optically black surface allows measurements of the dark current. The rotating wheel has eight positions located 45° apart, and data are acquired sequentially for each of the eight positions. A complete turn of the wheel is accomplished in 1.2 s, and the scanner rotates at a speed of 45°/min. (In 1.2 s the viewing zenith angle changes by ~1°.)

Table 2. Characteristics of Refpol

Parameter	Value
Wavelengths (bandwidths)	443, 550, 665, 870 nm (20, 40, 20, 40 nm)
Detector	Silicon photodiode
Dynamic range	1–500,000 NC[a]
Noise	±50 NC[a]
Integration time	16 ms
Field of view	2°
Cadence of measurements	1.2 s
Rotation rate	0.125 rpm

[a]NC, numerical counts.

If L_1, L_2, and L_3 denote the three components (specific intensities) of the polarization vector measured by Refpol (Fig. 7), the sequence of measurements is given in Table 3. One can see that, for each filter, L_1, L_2, and L_3 are not acquired simultaneously. To minimize errors, only consecutive acquisitions of L_1, L_2, and L_3 are used. A complete data set (i.e., three intensities and an optical zero for all filters) is obtained in ~0.5 s.

The incident radiance is partially polarized and can

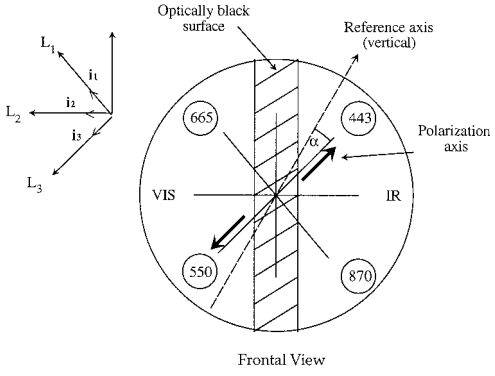

Fig. 7. Rotating wheel characteristics: two polarizers (VIS for 443, 550, and 670 nm and IR for 870 nm) and an optically black area. In the depicted configuration, L_3 is acquired at 550 nm and L_1 at 670 and 870 nm. Data at 443 nm are rejected because the polarizer sheet is not in the right position (443 nm must correspond to VIS).

Table 3. Sequence of Refpol Measurements for the Eight Positions of the Rotating Wheel

	Wavelength (nm)			
Position	443	550	665	870
1	—	L_3	L_1	L_1
2	0	0	L_2	L_2
3	L_1	—	L_3	L_3
4	L_2	—	0	0
5	L_3	—	—	—
6	0	0	—	—
7	—	L_1	—	—
8	—	L_2	0	0

Table 4. Refpol Calibration Coefficients in Reflectance Units ($\times 10^6$)

Date	Place	Method	Wavelength (nm) 443	550	665	870
09/25/96	LOA	Sphere	3.58	2.25	1.30	1.67
10/04/96	BSI[a]	Plaque	3.44	2.26	1.30	
04/08/96	SIO Pier	Plaque	3.57	2.22	1.34	1.92
11/25/96	LOA	Sphere	3.51	2.29	1.31	1.70
		Mean	3.53	2.25	1.32	1.76
	Standard deviation/mean (%)		±1.8	±1.2	±1.6	±7.2

[a]Biospherical Instruments, Inc., San Diego.

be decomposed into natural and polarized components.[13] For Earth observations the approximation of linear polarization (no ellipticity) is accurate, hence commonly used (e.g., Ref. 14). With this approximation the orthogonal directions i_1, i_2, and i_3 (Fig. 6) define a system of axes in which the Stokes parameters of the incident wave can be written as

$$I = L_3 + L_1, \tag{10a}$$

$$Q = L_3 - L_1, \tag{10b}$$

$$U = 2L_2 - L_1 - L_3. \tag{10c}$$

When viewing the surface, the optical axis rotates in the vertical plane and the wave oscillates in the plane perpendicular to the optical axis, the axis of propagation. Since surface reflection induces horizontal polarization, it is convenient to express the Stokes parameters in another base, with the axes parallel and perpendicular to the viewing plane. The angle between the optical axis of the polarizers and the reference axis is denoted by α (see Fig. 7). When the rotating axis is horizontal, the reference axis is the horizontal direction. In the new base the Stokes parameters become

$$I' = I, \tag{11a}$$

$$Q' = Q\cos(2\alpha) + U\sin(2\alpha), \tag{11b}$$

$$U' = -Q\sin(2\alpha) + U\cos(2\alpha), \tag{11c}$$

and the parallel (vertical) and perpendicular (horizontal) components of the incident radiance are

$$L^{//} = (I' + Q')/2, \tag{12a}$$

$$L^{\perp} = (I' - Q')/2. \tag{12b}$$

Thus, by measuring L_1, L_2, and L_3, one can obtain $L^{//}$ and $L^{\perp}$, hence the total radiance $L^{//} + L^{\perp}$ from Eqs. (10)–(12).

B. Radiometric Calibration

Refpol was radiometrically calibrated in the laboratory at LOA, Lille, France, and at Biospherical Instruments, Inc., San Diego. At LOA the instrument was placed at the entrance of an integrating sphere delivering a known spectral radiance. At Biospherical Instruments Inc., the instrument viewed at 45° a Spectralon plaque illuminated by a lamp of known spectral irradiance. The spectral radiance reflected from the plaque was calculated as the product of the bidirectional reflectance of the plaque ($\geq$0.983 for the viewing angle considered) and the spectral irradiance from the lamp.

A second type of calibration was performed in the field, at the SIO pier, La Jolla. Refpol was positioned vertically above a Spectralon plaque illuminated by the Sun in clear sky conditions. The reflectance of the plaque was greater than 0.990, and the incident solar irradiance on the plaque was calculated by using the successive orders of scattering code of Deuzé *et al.*[11] The spectral aerosol optical thickness, an input parameter to the code, was measured by a CIMEL Electronique sunphotometer (see below). The effect of the coast and pier on the diffuse irradiance reaching the plaque was negligible.

In Table 4 we give the calibration coefficients obtained by the various methods. For convenience the calibration coefficient K is computed in reflectance units as

$$\rho = \frac{\pi L}{E_{so}} = K(NC - NC_0), \tag{13}$$

where L is the given radiance reflected by the plaque used for calibration, NC is the measured numerical count, and NC_0 is the measured dark current count. Using this definition, we convert the field data NC_i corresponding to the polarization state $i(i = 1, 2, 3)$ into reflectances ρ_i by using

$$\rho_i = \frac{K(NC_i - NC_{0i})d^2}{\cos(\theta_s){d_0}^2}. \tag{14}$$

Note that the extraterrestrial solar irradiance does not appear explicitly in Eq. (14) because the calibration coefficients for ρ (Table 4) are already normalized for mean extraterrestrial solar irradiance. We finally transformed ρ_i into perpendicular- and parallel-polarized components, $\rho^{//}$ and $\rho^{\perp}$, by using Eqs. (10)–(12).

A total of four calibrations was performed, three in the laboratory and one in the field. Note that no value is reported at 870 nm for the Biospherical In-

struments Inc. calibration because the lamp used was not well characterized at that wavelength. The agreement is good between laboratory and field calibration coefficients, except at 870 nm. Standard deviations are between ±1% and 2% at 443, 550, and 665 nm but ±7% at 870 nm. Since no temporal trend can be detected in the calibration coefficients, average values were used in our study.

The sunphotometer had interference filters centered at 440, 670, 870, and 1020 nm and was radiometrically calibrated on 11 April 1996 at Stephenson Peak, Laguna Mountains (1896-m altitude) with the Bouguer–Langley method. The site was atmospherically stable, with negligible aerosols, making a determination of the calibration coefficients accurate. Note that aerosol optical thickness data are necessary not only for the SIO pier calibration of Refpol but also for normalization of the Refpol measurements and correction of skylight reflection effects.

C. Measurements

Refpol measurements were made on 8 and 10 April 1996 at the SIO pier. The radiometer was installed on a horizontally rotating boom at the south end of the pier, ~10 m above the sea surface. This setup allowed for selection of various relative azimuth angles between Sun and view directions. Data were collected in the solar plane (180°), in the plane at 135° from the solar plane, and in the plane perpendicular to the solar plane (90°). For each of these planes, Refpol scanned the sea surface from horizon to horizon. One scan was accomplished in 4 min.

The sky was partly cloudy during 8 and 10 April with cumulus or stratocumulus clouds or both, but cloud cover did not exceed a few octas. (The sky is divided into two parts, high and low, of four equal octas.) Data acquired when the Sun disk was obscured by the clouds were systematically discarded. Sunphotometer measurements were made when the Sun disk was free of clouds and were processed into aerosol optical thickness by standard techniques. The average optical thickness at 870 nm was 0.06 ± 0.01 and 0.18 ± 0.01 on 8 and 10 April and the angström coefficient between 440 and 870 nm was 1.18 ± 0.07 and 1.12 ± 0.05, respectively. These values for the angström coefficient are characteristic of continental aerosols often encountered at the coastal site of La Jolla.[15]

Owing to a red tide, the amount of phytoplankton was high during the Refpol measurements, giving the ocean a dark appearance. In fact, chlorophyll-*a* concentration was ~45 mg m^{-3} on 9 April.[16] Wind was light and waves were 0.2–0.5 m high at the end of the pier. The waves were not breaking, and there was no foam on the ocean surface.

D. Polarized and Total Reflectances

In Fig. 8 the parallel-polarized and total reflectances in the four spectral bands of Refpol are displayed as a function of viewing zenith angle. The Sun zenith angle is 27°, and the relative azimuth angle is 180°. The viewing zenith angles correspond to the back-

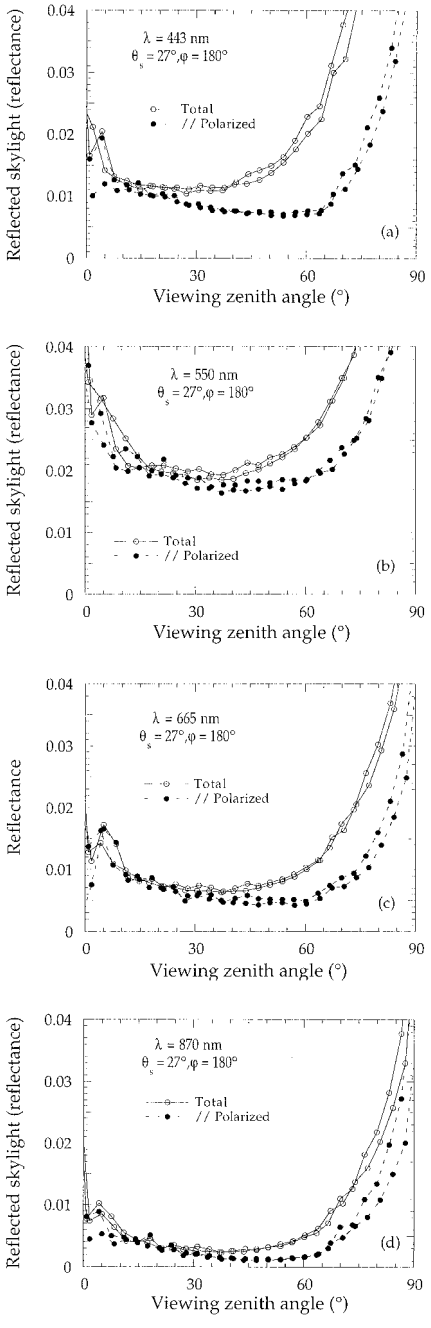

Fig. 8. Above-water Refpol measurements of parallel-polarized (dots) and unpolarized (circles) reflectances as a function of the viewing zenith angle for four wavelengths (443, 550, 665, and 870 nm). The solar zenith angle is 27°, and the relative azimuth angle is 180°. Two successive scans separated by ~4 min are presented. The measurements were performed at the SIO pier on 8 April 1996 at 18H55 Greenwich mean time (GMT).

scattering half-plane. Two consecutive scans, separated by ~4 min, are presented. Despite the nonsimultaneity of the measurements (spectral bands, polarization states) the consecutive scans exhibit consistent variations as well as spectral features except at low viewing zenith angles where glitter effects become important. As indicated by theory (see Section 2) the parallel-polarized reflec-

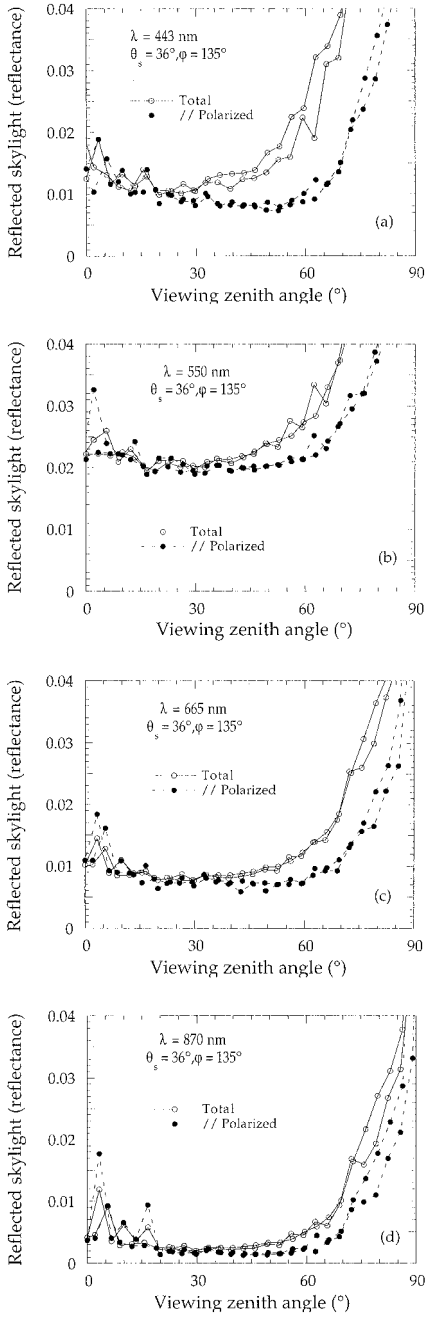

Fig. 9. Same as Fig. 8, but for a relative azimuth angle of 135° and for a solar zenith angle of 36°. The measurements were performed on 10 April 1996 at 17H53 GMT.

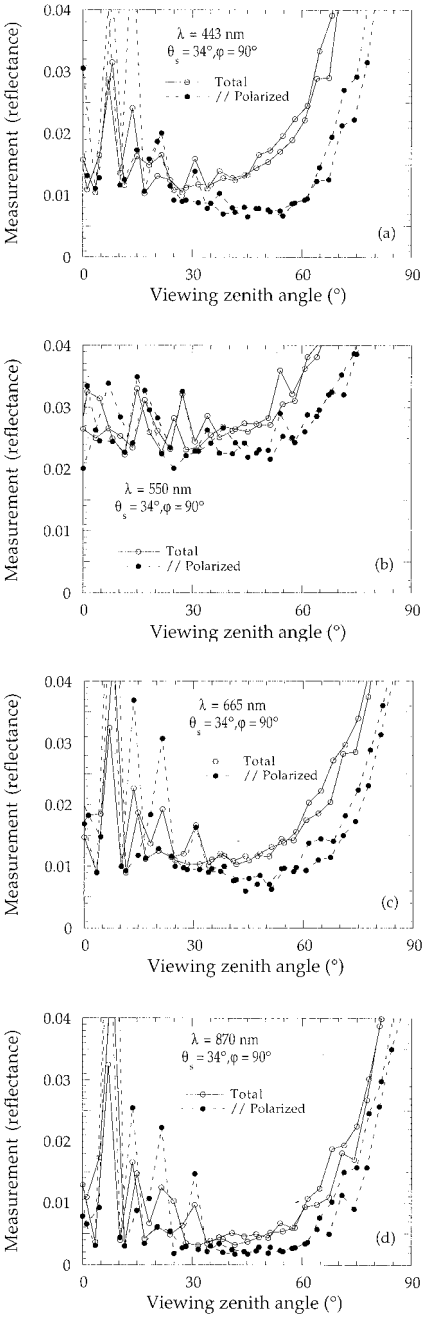

Fig. 10. Same as Fig. 8 but for a relative azimuth angle of 90° and a solar zenith angle of 34°. The measurements were performed on 10 April 1996 at 18H04 GMT.

tance is much smaller than the total reflectance at viewing angles near the Brewster angle, especially in the 443-nm spectral band (a factor of 2 smaller). Unlike the simulations presented in Section 2 (Figs. 1–5) the measurements include the signal backscattered by the water body, resulting in higher reflectances (Fig. 8). A similar dependence with viewing zenith angle is obtained when the relative azimuth angle is 135° instead of 180° (Fig. 9). The glitter effect, however, is more pronounced at higher viewing zenith angles (until ~30°), even through the solar zenith angle in Fig. 9 is higher than the one in Fig. 8 (36° instead of 27°). Surface roughness, however, although generally similar, was not strictly the same on 8 April (Fig. 8) and 10 April (Fig. 9). The glitter effect is especially apparent at 870 nm, where molecular scattering becomes small, in agreement with theory. Skylight reflection in the parallel-polarized component is also reduced dramatically near the Brewster angle, the reduction being more pronounced at the shorter wavelengths where the diffuse atmospheric transmittance is larger.

When the relative azimuth angle is changed to 90° (Fig. 10), the glitter influence is felt strongly below an

~40° viewing zenith angle. Figures 9 and 10 are directly comparable because the Refpol measurements were made on the same day at approximately the same time (the solar zenith angle changed only by 2°). The minimum of parallel-polarized reflectance near the Brewster angle is well defined and appears to occur over a shorter range of viewing zenith angles than the range for the cases of 135° and 180° relative azimuth angles, as predicted by theory. Because of the glitter effects, it is difficult to make measurements of total diffuse marine reflectance at viewing zenith angles below 40° in the vertical plane perpendicular to the solar plane. The viewing geometry selected by Carder and Steward[5] and Lee *et al.*[6,8] therefore is not optimum; it would be easier to correct glitter contamination in the measurements by viewing the surface at relative azimuth angles greater than 90°.

In Fig. 11 Refpol measurements again are displayed as a function of the solar zenith angle but for a higher solar zenith angle, 55°. Both the parallel-polarized and total reflectances do not increase with decreasing viewing zenith angle, as in the case of a solar zenith of 36° (Fig. 8). The glitter effect is minimal, and the variations with viewing zenith angle are smooth, except at 550 nm where some unexplained fluctuations in the signal occurred below a 50° viewing zenith angle, perhaps due to some instrumental malfunction or some inadvertent, yet brief, displacement of the boom during the measurements. At 443 nm the parallel-polarized reflectance slightly decreases with increasing viewing zenith angle, in agreement with theory (see Fig. 2), and there is again a substantial reduction in sky reflection near the Brewster angle. At 665 and 870 nm the parallel-polarized and total reflectances are constant below a 40° viewing zenith angle, and they have approximately the same value. Thus, when the solar zenith angle is high, there is no significant advantage in using a polarizer. Even viewing the surface vertically would be acceptable, although it might pose some practical problems with a handheld radiometer.

E. Derived Diffuse Marine Reflectance

The diffuse marine reflectance was derived from the Refpol scans by using Eqs. (7a) and (7b). It was assumed in the derivation that the diffuse marine reflectance ρ_w^{+} is Lambertian and unpolarized. This assumption is wrong and is discussed below. The atmospheric transmittance t_a in Eqs. (7a) and (7b) was computed for a molecular atmosphere, neglecting the aerosol's contribution justified by the low level on aerosol loading (see Subsection 3.C). However, no correction was affected to account for the presence of clouds that increase atmospheric transmittance when the Sun is not obscured by clouds. This effect is small when cloud coverage is only a few octas, the conditions of the experiment. In addition, for each Refpol measurement the total and parallel-polarized skylight reflection terms, ρ_c and $\rho_c^{//}$, were computed for a molecular atmosphere and in the absence of glitter (because wind speed was unknown during the measurements).

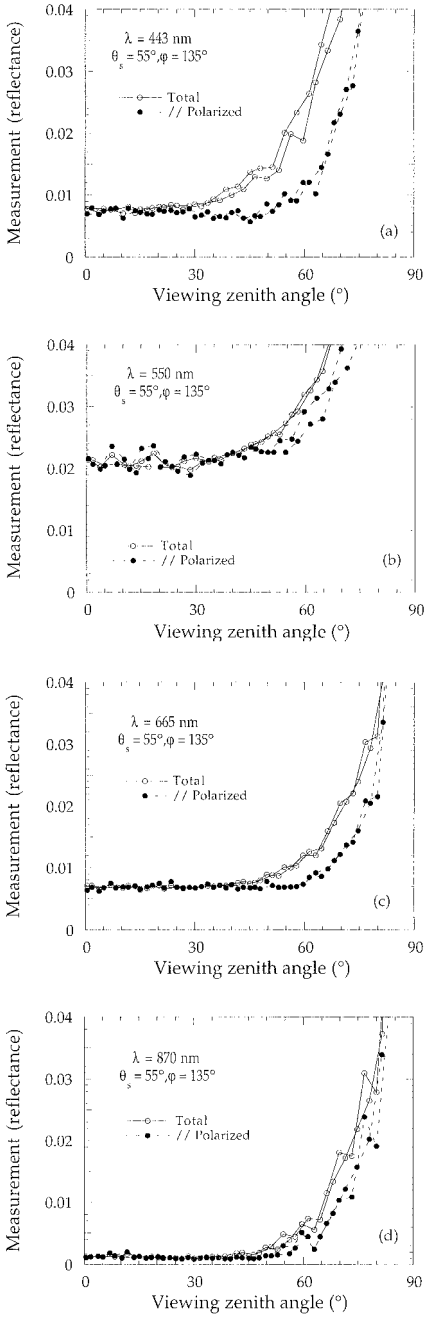

Fig. 11. Same as Fig. 8 but for a relative azimuth angle of 135° and a solar zenith angle of 55°. The measurements were performed on 8 April 1996 at 23H23 GMT.

Figure 12 gives examples of the derived marine reflectance at the four wavelengths after the above processing was done. The derived marine reflectance is plotted versus the viewing angle for parallel-polarized and unpolarized measurements. Unpolarized measurements have been treated in the same way as parallel-polarized measurements, i.e., by computing and subtracting the skylight reflection effects and dividing by the atmospheric total transmittance for a molecular atmosphere. The geometry is character-

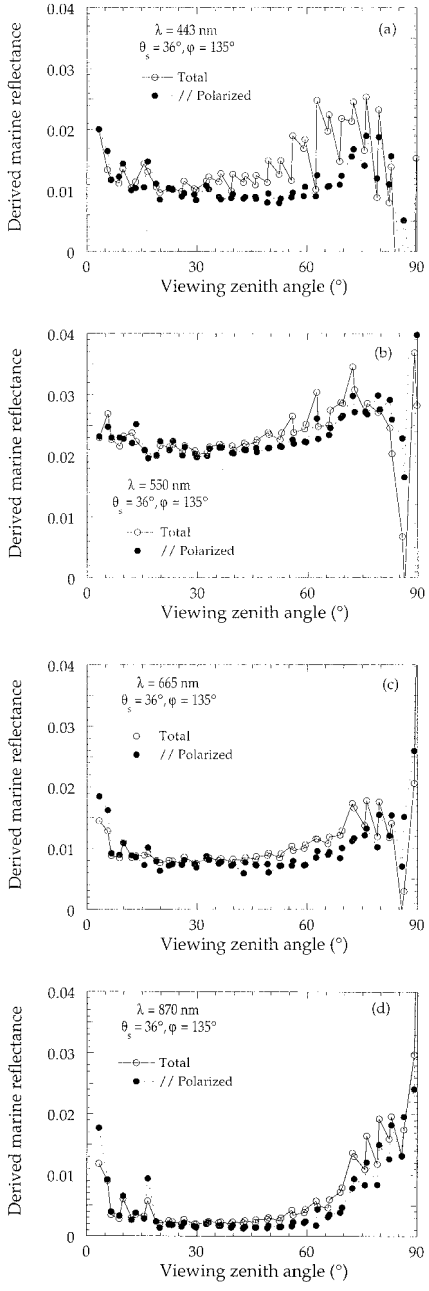

Fig. 12. Diffuse marine reflectance derived from the parallel-polarized (dots) and unpolarized (circles) Refpol measurements of Fig. 9 as a function of the viewing zenith angle for the four wavelengths [(a) 443 nm, (b) 550 nm, (c) 665 nm, and (d) 870 nm]. The solar zenith angle is 36° and the relative azimuth angle is 135°.

ized by a solar zenith angle of 36°, and the corresponding above-water measurements are those in Fig. 9. The effect of glitter is obvious when one is viewing close to nadir. One should observe a constant value of the diffuse marine reflectance if it were Lambertian and if the skylight reduction were perfect. This result is obviously not the case for viewing zenith angles greater than 60°. Viewing at these angles and at nadir should be definitively excluded. Using parallel-polarized measurements, we obtain a stable estimate of the diffuse marine reflectance at viewing zenith angles between approximately 30° and 60° viewing angles, so it seems that there is some flexibility in the choice of viewing conditions around the Brewster angle. For unpolarized measurements the correction is much less accurate, and this accuracy decreases at shorter wavelengths, especially 443 nm, for which the skylight radiation increases. The curves in Fig. 12 give the general visual impression that (1) the estimate of the diffuse marine reflectance is the same when the two methods are used and (2) the estimate of the diffuse marine reflectance is easier and more accurate when parallel-polarized measurements are used rather than unpolarized ones.

Around the Brewster viewing angle the measured reflectance is ~0.007 at 443 nm, 0.022 at 550 nm, 0.006 at 665 nm, and ~0.001 at 870 nm. For comparison in oligotrophic waters the diffuse marine reflectance of the water body may reach 0.03 at 443 nm, ~0.003 at 550 nm, and nearly zero at 665 and 870 nm (e.g., Refs. 17 and 18). The small signal observed in the 443-nm spectral band and the significant signal observed at longer wavelengths in the visible are explained by the presence of a red tide during the Refpol measurements and may also be due to, mainly in the 870 nm spectral band, the presence of small clouds that can modify the atmospheric diffuse transmittance approximated by Eq. (9).

Table 5. Mean and Standard Deviation of Marine Reflectance Estimated from the Above-Water Refpol Measurements

	Wavelength (nm)		
Date	443	550	665
04/08/96[a]	0.0080 ± 0.0013	0.0215 ± 0.0028	0.0061 ± 0.0015
04/10/96[a]	0.0073 ± 0.0010	0.0214 ± 0.0015	0.0077 ± 0.0008

[a]From approximately 20 to 24 UT.

F. Comparison with Underwater Measurements of Marine Reflectance

Concomitant with the Refpol measurements, vertical profiles of downwelled irradiance and upwelled radiance in spectral bands centered at 443, 555, and 665 nm were obtained with an underwater instrument, the MER radiometer.[19] Diffuse marine reflectances were computed as the ratio of upwelled radiance and downwelled irradiance, measured at different depths and extrapolated to the surface. Tables 5 and 6 give the mean and the standard deviation of the diffuse marine reflectances derived from the Refpol and the

Table 6. Mean and Standard Deviation of Marine Reflectance Measured by the Underwater MER Radiometer

	Wavelength (nm)		
Date	443	555	665
04/08/96[a]	0.0068 ± 0.0054	0.0237 ± 0.0145	0.0072 ± 0.0057
04/10/96[a]	0.0052 ± 0.0010	0.0183 ± 0.0129	0.0047 ± 0.0063

[a]The measurements were made at the same time as that of the Refpol radiometer.

MER measurements made during 8 and 10 April. Both underwater and above-water methods yield reflectances that are in general agreement with high values at 550 nm and low values at 443 and 665 nm. The standard deviation, an indicator of the repeatability of the measurements made by Refpol, is very small, ~0.001 in reflectance at 443, and 665 nm, where the skylight reflection correction is relatively large because of the low diffuse marine reflectances (0.006–0.007 at 443 and 665 nm). At 550 nm the higher variability of the diffuse marine reflectance derived from Refpol measurements (a standard deviation of above 0.003) can be attributed to a high-water-body signal. A comparison of standard deviations of the measurements made by the two radiometers suggests that Refpol measurements may be duplicated.

It is difficult to investigate the comparison further. Both the Refpol and the MER instruments measure directional reflectance, and the data should be normalized before comparison.[20] This was not done because of difficulties in this situation of a red tide. In addition the MER data were not corrected for instrument self-shadowing, and the effects may be substantial owing to the large phytoplankton concentration, hence absorption.[4] Furthermore, since the water body may polarize incident sunlight (e.g., Refs. 21–23), the polarized diffuse marine reflectance measured by Refpol is not exactly the total diffuse marine reflectance measured by the MER radiometer, in fact obtained in Eq. (7b), and this result can affect the comparison (see below).

G. Polarization of the Diffuse Marine Reflectance

As we measure the parallel-polarized component of the light scattered by the water body, we must be aware of an eventual bias due to polarization of the scattering. Even though polarization by ocean constituents is little known, except by water molecules, it is nevertheless possible to crudely estimate the effect. Let us assume that (1) incident solar irradiance is only direct, (2) the main source of polarization is molecular scattering, with no depolarization factor, and (3) water absorption is large enough so that multiple scattering can be neglected. Then we can easily obtain the maximum effect of polarization, i.e., the ratio α_{pol} of estimates of $\rho_w{}^+$ by using parallel-polarized and unpolarized measurements. For the Sun at zenith we have

$$\alpha_{\mathrm{pol}} = \frac{2\cos^2\chi}{(1+\cos^2\chi)}, \tag{15}$$

where χ is the underwater scattering angle. At lower Sun elevations the scattering and viewing planes are no longer coincident, and Eq. (15) approximates only the actual polarization factor. For the geometry under consideration, i.e., the viewing zenith angle of 45° and the relative azimuth angle of 135°, the underwater scattering angle varies between only 148° and 158°, and thus the maximum polarization factor α_{pol} varies from 0.83 to 0.92. Obviously more precise computations are necessary to assess polarization effects better. The α_{pol} values provided here are only rough estimates. However, we should be able to correct the effects with good accuracy, say, ±5% relative accuracy, which compares with other errors, such as those due to bidirectional effects and radiometric calibration errors.

4. Conclusions

The theoretical calculations presented in Section 2 have shown that reflected skylight in the field of view of a radiometer viewing the ocean surface from above can be reduced substantially by using a vertical polarizer, i.e., by measuring the polarized component of the reflectance in the viewing plane. For maximum reduction of skylight reflection effects, the measurements must be made near the Brewster angle, at an ~135° viewing zenith angle and at relative azimuth angles greater than 90°. In this configuration, reflected skylight can be reduced to typically 10^{-3} at 443 nm. This represents 2–10% of the diffuse marine reflectance, the signal of interest. Furthermore the effects of surface roughness on skylight reflection, hence uncertainties in the sea state (wind speed), are minimized. Taking into account typical uncertainties of wind speed and geometry, we may correct the residual reflected skylight to a few 10^{-4} in reflectance units. We verified experimentally the theoretical results at the SIO pier by viewing the ocean surface with the Refpol radiometer. The various angular and spectral effects predicted by theory have been evidenced in the measurements.

In the study of Lee *et al.*[8] the use of a vertical polarizer did not improve the measurements of diffuse ocean reflectance. Our theoretical and experimental results indicate that for a viewing zenith angle of 30° and a relative azimuth angle of 90°, i.e., the geometry selected by Lee *et al.*,[8] the parallel-polarized and total skylight reflection signals are nearly the same. In other words the reduction of skylight reflection effects, substantial near the Brewster angle, becomes nil for a viewing zenith angle of ~30°.

In view of the theoretical and the experimental results discussed above, one can make the following recommendations for measuring diffuse ocean reflectance from above the surface.

First, to minimize surface reflection effects that are generally important at low solar zenith angles, a vertical polarizer may be used, and the surface must be viewed at 45° from zenith (near the Brewster angle) and at a relative azimuth angle of 135°. Measuring at larger relative azimuth angles is acceptable but might be difficult from a ship (because of shadow effects). The recommended configuration is more practical, making it easy to perform measurements with a handheld instrument on any platform at sea including moving ships. Furthermore, when the relative azimuth angle is increased to 180°, the diffuse marine reflectance is increasingly sensitive to the backward peak of the phytoplankton phase function, whose magnitude is generally unknown yet variable,

and making angular corrections to match the viewing geometry of a satellite ocean color sensor, or using the data to develop bio-optical algorithms, becomes difficult.

Second, a spectral band in the near-IR where the ocean is black (e.g., 865 nm) would help detect and correct eventual cloud and whitecap effects, even residual sun glint, with the assumption in a first approximation that the effects are spectrally white.

Third, measurements without a polarizer should not be made perpendicular to the solar plane but at a relative azimuth angle greater than 90° (e.g., 135°), so that the effects of sun glint and skylight reflection can be reduced at low solar zenith angles. A 30° viewing angle is adequate in this case, since the surface reflection effects are minimum at this angle or not a problem (when the solar zenith angle is high). If a relative azimuth angle of 90° is used, a viewing zenith angle of 40° is preferred.

This research has been supported by the Centre National d'Etudes Spatiales, the Centre National de la Recherche Scientifique, the Région Nord-Pas-de-Calais, and the NASA contract NAS5-97135 (to R. Frouin) and grant NAG5-6202 (to R. Frouin). We thank B. G. Mitchell, M. Kahru, and T. Moisan from the SIO for providing phytoplankton concentration and diffuse marine reflectance data and J. McPherson from SIO for programming support.

References

1. M. Viollier, "Radiometric calibration of the Coastal Zone Color Scanner on Nimbus-7: a proposed adjustment," Appl. Opt. **21,** 6142–6145 (1982).
2. D. K. Clark, H. R. Gordon, K. J. Voss, Y. Ge, W. Broenkow, and C. Trees, "Validation of atmospheric correction over the oceans," J. Geophys. Res. **102,** 17,209–17,217 (1997).
3. B. Fougnie, P. Y., Deschamps, and R. Frouin, "Vicarious calibration of the POLDER ocean color spectral bands using *in situ* measurements," IEEE Trans. Geosci. Remote Sensing, ADEOS special issue, **37,** 1567–1574 (1998).
4. J. L. Mueller and R. W. Austin, "Ocean optics protocols for SeaWiFS validation, Revision 1," SeaWiFS Tech. Rep. Series (NASA, Goddard Space Flight Center, Greenbelt, Md., 1995).
5. K. L. Carder and R. G. Steward, "A remote-sensing reflectance model of a red tide dinoflagellate off West Florida," Limnol. Oceanogr. **30,** 286–298 (1985).
6. Z. P. Lee, K. L. Carder, R. G. Steward, T. G. Peacock, C. O. Davis, and J. L. Mueller, "Remote sensing reflectance and inherent optical properties of oceanic waters derived from above-water measurements," in *Ocean Optics XIII*, S. G. Ackleson and R. Frouin, eds., Proc. SPIE **2963,** 160–166 (1997).
7. K. L. Carder, P. Reinersman, R. F. Chen, F. Muller-Karger, C. O. Davis, and M. Hamilton, "AVIRIS calibration and application in coastal oceanic environments," Remote Sens. Environ. **44,** 205–216 (1993).
8. Z. P. Lee, K. L. Carder, T. G. Peacock, and R. G. Steward, "Remote-sensing reflectance measured with and without a vertical polarizer," in *Ocean Optics XIII*, S. G. Ackleson and R. Frouin, eds., Proc. SPIE **2963,** 483–488 (1997).
9. P. Koepke, "Effective reflectance of oceanic whitecaps," Appl. Opt. **23,** 1816–1824 (1984).
10. C. Cox and W. Munk, "Measurements of the roughness of the sea surface from photographs of the sun's glitter," J. Opt. Soc. Am. **44,** 11,838–11,850 (1954).
11. J. L. Deuzé, M. Herman, and R. Santer, "Fourier series expansion of the transfer equation in the atmosphere–ocean system," J. Quant. Spectrosc. Radiat. Transfer **41,** 6483–6494 (1989).
12. P. Y. Deschamps, M. Herman, and D. Tanre, "Modeling of the atmospheric effects and its application to the remote sensing of ocean color," Appl. Opt. **22,** 3751–3758 (1983).
13. S. Chandrasekhar, *Radiative Transfer*, (Oxford University, Oxford, England, 1950; Dover, New York, 1960).
14. J. Lenoble, *Atmospheric Radiative Transfer*, (A. Deepak, Hampton, Va., 1993).
15. M. Schwindling, P. Y. Deschamps, and R. Frouin, "Validation of aerosol models for satellite ocean color remote sensing," J. Geophys. Res. **103,** 24,919–24,935 (1998).
16. T. Moisan and B. G. Mitchell, Scripps Institution of Oceanography, 9500 Gilman Drive, La Jolla, California (personal communication, 1997).
17. A. Morel, "Optical modeling of the upper ocean in relation to its biogenous matter content (case 1 waters)," J. Geophys. Res. **93,** 10,749–10,768 (1988).
18. A. Morel, "Optical properties of oceanic case 1 waters, revisited," in *Ocean Optics XIII*, S. G. Ackleson and R. Frouin, eds., Proc. SPIE **2963,** 108–114 (1997).
19. B. G. Mitchell and M. Kahru, Scripps Institution of Oceanography, 9500 Gilman Drive, La Jolla, California (personal communication, 1997).
20. A. Morel and B. Gentili, "Diffuse reflectance of oceanic waters 2: bidirectional aspects," Appl. Opt. **32,** 6864–6879 (1993).
21. A. Ivanoff, *Introduction à l'océanographie: Tome II*, (Vuibert, Paris, 1975).
22. K. Masuda and T. Takashima, "Dependence of the radiation just above and below the ocean surface on atmospheric and oceanic parameters," Appl. Opt. **27,** 4891–4898 (1988).
23. R. Frouin, E. Pouliquen, and F.-M. Bréon, "Ocean color remote sensing using polarization properties of reflected sunlight," in *Proceedings of the Sixth International College on "Physical Measurements and Signatures in Remote Sensing*," 17–21 January 1994, Val d'Isère, France, ISPRS. 665-674 (Centre National d'Etudes Spatiales, Toulouse, France, 1994).